

# Progenitors of type Ia supernovae and the metallicity distribution of G-type dwarfs

N. Mennekens<sup>1</sup>, D. Vanbeveren<sup>1,2</sup>, and J.P. De Greve<sup>1</sup>

<sup>1</sup> Astrophysical Institute, Vrije Universiteit Brussel, Pleinlaan 2, 1050 Brussels, Belgium  
e-mail: nmenneke@vub.ac.be

<sup>2</sup> Groep T - Leuven Engineering College, KU Leuven Association, Andreas Vesaliusstraat 13, 3000 Leuven, Belgium

Received 16 November 2012

## ABSTRACT

**Aims.** We investigate the contribution to the formation of type Ia supernovae of the single (a white dwarf accreting from a non-degenerate companion) and double (two merging white dwarfs) degenerate scenario, as well as various aspects of the binary evolution process leading to such a progenitor system.

**Methods.** We use the combination of a population synthesis code with detailed binary evolution and a galactic chemical evolution model to predict the metallicity distribution of G-type dwarfs in the solar neighborhood. Because of the very long lifetime of these stars, this distribution is a good indicator of the entire chemical history of a region. By comparing the observed distribution with those predicted by assuming different type Ia supernova progenitors and evolutionary parameters (e.g. concerning mass and angular momentum loss and common envelope evolution), it is possible to constrain the possible combinations of assumptions.

**Results.** We find that in order to reproduce the observed G-dwarf metallicity distribution, it is absolutely necessary to include both the single and double degenerate scenario. The best match is obtained when all merging C-O white dwarfs contribute to the latter. The correspondence is also critically dependent on the assumptions about galaxy and star formation, e.g. the use of the two-infall model vs. a constant star formation rate. However, this does not affect the previous conclusion, which is consistent with the results obtained by investigating type Ia supernova delay time distributions in starburst galaxies.

**Key words.** supernovae: general – binaries: close – stars: white dwarfs – galaxies: starburst – Galaxy: abundances – Galaxy: evolution – Galaxy: solar neighborhood

## 1. Introduction

Type Ia supernovae (SNe Ia), the most powerful events produced by nature, are not only of critical importance as cosmological distance indicators (cf. the 2011 Nobel Prize in Physics), but also for the chemical enrichment of galaxies. A large fraction of all iron in the solar neighborhood is known to have been produced by these events. It is commonly agreed upon that SNe Ia originate from white dwarfs (WDs) that exceed a critical mass and as a result undergo a thermonuclear disruption. Many things remain unclear however: whether this happens at the Chandrasekhar mass or above or below, whether only carbon-oxygen (C-O) WDs qualify, whether the disruption is a deflagration or detonation, etc. Perhaps most strikingly, even the type of progenitor system remains uncertain (see Maoz & Mannucci 2012, for a review). Since the WD needs to accrete in order to reach the critical mass, it is obvious that only interacting (i.e. binary or multiple) stars can produce such events. However, many different scenarios for the accretion process have been proposed. The most popular ones are known as the single degenerate (SD) and double degenerate (DD) scenario. In the SD scenario (see e.g. Whelan & Iben 1973; Nomoto 1982), one WD accretes from a late main sequence (MS) or red giant (RG) companion. The mass transfer rate towards the WD is of critical importance for the scenario to work: if it is too high, the WD will suffer from a RG-like expansion, if it is too low, the WD will burn the acquired mass in classical nova outbursts and will never attain the required critical mass to explode. Hence, a commonly invoked mechanism to explain such a moderate rate is a stabilizing wind from the WD. In

the DD scenario (see e.g. Iben & Tutukov 1984; Webbink 1984), the explosion is the result of the merger of two WDs, coming together due to the emission of gravitational wave radiation (GWR). In the case of unequal masses, the least massive of the two will be tidally disrupted and accreted by the more massive one, which is thus allowed to reach the critical mass. It has been previously suggested that such an event would lead to an accretion induced collapse resulting in a neutron star (NS), and not a SN Ia. However, Piersanti et al. (2003) showed that the inclusion of the effects caused by rotation may well solve this problem. Recent studies also consider the possibility of subluminal SNe Ia from equal mass C-O WD mergers (Pakmor et al. 2010), perhaps even below the Chandrasekhar mass (van Kerkwijk et al. 2010). In the DD scenario, one thus needs a double WD binary with a small orbital separation, so that GWR will sufficiently reduce the distance between the stars within the Hubble time. While it is conceivable that due to the nature of most scenarios the explosion mass is always similar, it is very important to address the question of the explosion mechanism, not in the least given the mentioned importance as “standard candles” in cosmology.

Many methods have been attempted to discriminate between both scenarios and hence to determine which (or both) of them generates SNe Ia in nature (again, see Maoz & Mannucci 2012, for an overview). It then concerns the study of whole populations and of individual explosions, both historic (e.g. Schaefer & Pagnotta 2012) and contemporary (e.g. Chomiuk et al. 2012, for SN 2011fe). A promising method on a global population scale is the study of the delay time distri-

bution (DTD), the response function giving the number of SNe Ia as a function of time after an instantaneous starburst. DTDs can be observationally measured in passively evolving (elliptical) galaxies, and theoretically computed with population synthesis codes, assuming different SN Ia progenitor channels. A comparison of the two then allows to constrain the formation models.

This paper does not address the physical (im)possibility of either formation scenario, but assumes that both of them may work as described by their various authors. From this premise, it is then investigated what scenario (or both) best theoretically reproduces population properties that can be observationally tested, also depending on various other evolutionary assumptions and parameters, both stellar and galactic.

Comparing the observed DTDs of SNe Ia in passively evolving starburst galaxies to those obtained under various assumptions with a population synthesis code, Mennekens et al. (2010) (hereafter M10) showed that the SD scenario alone can not account for the amount of SNe Ia required at more than a few Gyr after starburst. Furthermore, it was found that most DD SN Ia progenitors undergo a phase of stable, quasi-conservative Roche lobe overflow (RLOF) followed by a common envelope (CE) phase, as opposed to two successive CE phases. Finally, stellar rotation was proposed to mitigate the discrepancy between the absolute number of events predicted and those observed.

M10 also made a comparison with DTDs previously obtained by other groups using population synthesis methods. The preliminary conclusion was that on many points, a good agreement was found with most of them, however only under the obvious but challenging condition that the assumptions of the other groups were reproduced as much as possible. It was already hinted that, apart from initial distributions, the most important differences in assumptions would be those about mass and angular momentum loss, as well as the treatment of CE phases. Since then, it has become clear to the population synthesis community that it is indeed necessary to investigate the differences in the predictions made by different groups, and to look for the causes thereof. Currently, a joint explanatory paper by four groups working on the delay times of SNe Ia by means of population synthesis codes is in preparation (Toonen et al. 2013). In that study, the groups behind the studies of Claeys et al. (2010), Ruiter et al. (2011), Toonen et al. (2012), as well as this one, homogenized their codes as much as technically possible, and showed that this does indeed cause the predictions to converge toward one another. This work has indeed shown that the most flagrant discrepancies (which are evident when one compares theoretical DTDs, especially SD, produced by different groups with their own assumptions) are being caused by differences in the assumptions on these three most critical topics (mass loss, angular momentum loss, and CE evolution). However, it has also become clear that some (more minor) differences cannot be explained by different parameterizations, but are the result of inherent differences in the code, i.e. differences in the “single star tracks”, the evolution tracks of individual binary components. This is of course to be expected, given the very different ways population codes can be conceived, e.g. with the analytical formalisms by Hurley et al. (2002) vs. the use of full binary evolution, including the effects of accretion induced full mixing in stars that accrete from their companion through an accretion disk (see further). The influence of these differences on the macroscopic predictions relevant for this study will be discussed in Sect. 3.3.

This paper intends to confirm and extend the results of M10 by means of a method independent of the previous, i.e. not only

the number of SNe Ia at a certain time (the DTD), but their lasting legacy on the chemical history of a region. In addition, it does not limit itself to the study of passive elliptical galaxies, but aims to reproduce the chemical history and SN Ia rate of the solar neighborhood, in the actively evolving Milky Way Galaxy. Section 2 summarizes the most important elements contained in the used evolution codes, as well as the assumptions about binary evolution, SN Ia progenitors and the chemical evolution model. Section 3 then discusses the obtained results, while Sect. 4 summarizes the main conclusions.

## 2. Assumptions

### 2.1. The Brussels population synthesis code

The Brussels population synthesis code uses as input thousands of binary evolutionary calculations performed in detail with the Paczyński (1967) based Brussels binary evolution code. The latter, under development for over three decades, is extensively described in Vanbeveren et al. (1998a). The population code itself is elaborated in De Donder & Vanbeveren (2004). We repeat here only those elements that are of particular importance to this study. One of the most important consequences of using detailed binary evolution results in the population code is that the effects of accretion on the further evolution of the gainer star are treated in detail. To do this, it is assumed that when a star accretes by direct impact, this process occurs following the “snowfall” model by Neo et al. (1977). When, however, the orbital separation is sufficiently wide to lead to the occurrence of an accretion disk, it has been shown by Packet (1981) that the gainer star will relatively soon be spun up to (near-)critical rotation. Therefore, it is assumed that in such case the gainer star will be fully mixed, an event known as “accretion induced full mixing” (see Vanbeveren & De Loore 1994). Especially in this case, the further evolution of this star will be markedly different than if it would have been unaffected. Therefore, it is certainly not sufficiently accurate to estimate that the time needed to obtain an accreting WD or a double WD is simply equal to the nuclear lifetime of the least massive star. The binary evolutionary calculations themselves have been published by Vanbeveren et al. (1998b).

It is common in population synthesis codes to model many aspects of binary evolution by the use of parameters. This is necessary in order to be able to follow a large population of systems simultaneously, as is required in this study. Apart from initial distributions, the assumptions that most affect the results are those about mass loss, angular momentum loss, and the treatment of CE phases. Given the already mentioned wide variety of assumptions encountered in the literature, a small elaboration and explanation of our assumptions is in order.

The population code starts from a  $10^6 M_{\odot}$  starburst with a given binary frequency (the fraction of primaries that have a stellar companion) and metallicity  $Z$ . Primary star masses  $M_1$  are drawn from a Kroupa et al. (1993) initial mass function (IMF) normalized between 0.1 and  $120 M_{\odot}$ . Three different mass ratio distributions are considered: a flat one (as standard), one favoring high mass ratios (Garmany et al. 1980) and one favoring small mass ratios (Hogeveen 1992), all normalized to allow secondaries with a mass  $M_2$  between  $0.1 M_{\odot}$  and  $M_1$ . Reflecting the results of Abt (1983), the initial orbital period distribution is taken to be logarithmically flat, and is normalized between 1 day and 10 years.

Whenever the initially most massive star (subscript 1) in a binary fills its Roche lobe, this will initiate a mass transfer phase.

Depending on whether this happens during core H burning (case A), shell H burning (case B) or after core He burning (case C), the nature of this phase and the consequences for the binary system will be different.

In the event of case A or early case B (known as case Br, i.e. at a time when the donor's outer layers are still radiative), mass loss will lead to the star retreating within its Roche lobe, and therefore be self-mitigating. The result will be a dynamically stable stream of matter from donor to gainer. How much of this matter is actually accreted by the gainer star (subscript 2) is determined by the quantity  $\beta$ , defined by

$$\beta = \left| \frac{\dot{M}_2}{\dot{M}_1} \right|. \quad (1)$$

In the case of stable RLOF,  $\beta$  is equal to  $\beta_{\max}$ , which is a common parameter in most population synthesis codes. In our standard model,  $\beta_{\max} = 1$ , signifying that the donor accepts all matter lost by the donor. We obviously discuss the influence on the results of smaller values, and this discussion will indeed turn out to support a value close to 1 in reality.

Apart from changing the masses of both donor and gainer (except when  $\beta = 0$ ), another important consequence of mass transfer is a change in orbital period and thus separation. In the case of conservative mass transfer ( $\beta = 1$ ), this change is simply given by

$$\frac{P_f}{P_i} = \left( \frac{M_{1i}M_{2i}}{M_{1f}M_{2f}} \right)^3, \quad (2)$$

with subscripts i and f standing for initial and final with regard to the RLOF-phase. However, if  $\beta < 1$  an assumption is required about how much angular momentum is carried from the system by a given amount of mass loss. This comes down to specifying how and where the matter leaves the system. A commonly made assumption in population synthesis codes is that mass is lost with the specific orbital angular momentum of the gainer star. This is however only justified if the matter leaves the system in a way that is symmetric with respect to the equatorial plane of the gainer (e.g. through an enhanced stellar wind or bipolar jets). As there is limited evidence for significant mass loss in such a way in intermediate mass non-degenerate stars, our standard model is that matter will instead form a non-corotating circumbinary ring after passing through the second Lagrangian point  $L_2$ . In this case, the lost angular momentum is the specific orbital angular momentum of the disk, which is determined by its radius, and considerably larger than that of the gainer (since it is further from the center of mass). Hence, in our standard model, a given amount of mass loss will lead to a much larger angular momentum loss, and thus more systems that merge, than with the specific gainer orbital angular momentum loss. Obviously, we will also model the latter assumption. This can be done with the prescription proposed by Rappaport et al. (1983) (with  $A$  the orbital separation and  $P$  the orbital period):

$$\dot{J} = \sqrt{\eta} \dot{M}_1 (1 - \beta) \frac{2 \pi A^2}{P}, \quad (3)$$

where  $\eta$  is a parameter describing the angular momentum loss  $\dot{J}$ . Whenever it can be assumed that  $\eta$  is constant (implying that the location and manner through which matter is lost are constant) during the considered timeframe, the period evolution is given by (see e.g. Podsiadlowski et al. 1992):

for  $0 < \beta < 1$ :

$$\frac{P_f}{P_i} = \left( \frac{M_{1f} + M_{2f}}{M_{1i} + M_{2i}} \right) \left( \frac{M_{1f}}{M_{1i}} \right)^{3[\sqrt{\eta}(1-\beta)-1]} \left( \frac{M_{2f}}{M_{2i}} \right)^{-3[\sqrt{\eta}\frac{1-\beta}{\beta}+1]}; \quad (4)$$

for  $\beta = 0$ :

$$\frac{P_f}{P_i} = \left( \frac{M_{1f} + M_{2f}}{M_{1i} + M_{2i}} \right) \left( \frac{M_{1f}}{M_{1i}} \right)^{3(\sqrt{\eta}-1)} e^{3\sqrt{\eta}\left(\frac{M_{1f}-M_{1i}}{M_{2i}}\right)}. \quad (5)$$

In the case of mass loss through  $L_2$ , it was also shown by Soberman et al. (1997) that the value of  $\eta$  is fairly constant, and can be well approximated by  $\eta = 2.3$ . This value is based on the reasoning that smaller circumbinary ring radii (corresponding to smaller  $\eta$ ) will lead to fragmentation and fall-back of the ring due to tidal forces by an uneven potential. If specific gainer orbital angular momentum is assumed, it is straightforward to show that  $\eta = \left( \frac{M_1}{M_1 + M_2} \right)^4$ . This means however, that  $\eta$  continuously changes during mass transfer, and that Eqs. (4) and (5) are in principle not valid if applied in one step from the situation before to after RLOF. It has been checked however that the method of averaging  $\eta$  before and after the mass transfer phase (as is done in the population synthesis code) results in virtually the same result as fully integrating the period evolution.

If the mass ratio between the two stars is extreme ( $q = M_2/M_1 < 0.2$ ) at the onset of mass transfer, this will result in an instability (Darwin 1879). The donor star will be unable to extract sufficient angular momentum from the orbit to remain in synchronized rotation, resulting in the mass transfer episode quickly becoming dynamically unstable. Tidal interaction will cause the secondary to spiral into the donor's outer layers, a process that is treated identically to the unstable type of mass transfer described in the next paragraph. In this case, it is assumed that  $\beta = 0$  regardless of  $\beta_{\max}$ . To ensure continuity, a linear interpolation is used between  $q = 0.2$  ( $\beta = 0$ ) and  $q = 0.4$  ( $\beta = \beta_{\max}$ ).

When mass transfer starts at a time when the outer layers of the donor are deeply convective (case Bc or case C), mass loss will not cause the donor to shrink, but to expand. Therefore, its expansion will not be slowed down, and an unstable mass transfer phase will ensue. After a short time, the envelope of the donor will engulf the other star, and both will rotate within one common envelope. The viscous friction of both stellar cores within this envelope will cause a reduction of the orbital separation. Part of the lost orbital energy will be converted into kinetic energy which can be used to expel the common envelope. If this conversion is sufficiently efficient, the envelope may be ejected in time to allow a new binary with smaller orbital separation to emerge. If not, both stars will merge. Many different formalisms have been proposed to model the energy conversion. The most popular one is the  $\alpha$ -formalism by Webbink (1984), which assumes a conservation of energy to balance the angular momentum before and after the CE phase:

$$\frac{M_{1i}(M_{1i} - M_{1f})}{\lambda R_{\text{Roche}}} = \alpha \left( \frac{M_{1f}M_{2i}}{2A_f} - \frac{M_{1i}M_{2i}}{2A_i} \right). \quad (6)$$

In this formula,  $R_{\text{Roche}}$  is the Roche radius of the donor, while  $\lambda$  is determined by the density profile of this star's outer layers, and  $\alpha$  is the energy conversion efficiency. The latter two values are quite uncertain, and are in population synthesis context often combined into a single parameter  $\alpha\lambda$ . Our standard model takes  $\alpha\lambda = 1$  (as do most population synthesis studies), while other (mainly smaller) values are also considered.

Dewi & Tauris (2000) determined values for  $\lambda$  for different kinds of stars, mostly finding values well below unity. The Brussels code allows to assign a different value for  $\alpha\lambda$  to each system according to these results, and a run in this mode will be discussed. In recent studies, Davis et al. (2010) and Zorotovic et al. (2010) have determined values for  $\alpha$  also resulting in  $\alpha\lambda$  up to an order of magnitude below 1.

On the other hand, Nelemans et al. (2000) propose the  $\gamma$ -scenario, which conversely assumes a conservation of angular momentum to arrive at a balance of energy:

$$\frac{\Delta J}{J} = \gamma \frac{\Delta M_{\text{total}}}{M_{\text{total}}} = \gamma \frac{M_{1i} - M_{1f}}{M_{1i} + M_{2i}}, \quad (7)$$

the parameter  $\gamma$  in this equation having the same function of denoting conversion efficiency as  $\alpha$  in the other formalism. Based on observational constraints, the authors propose a value of  $\gamma = 1.5$ . This yields the following orbital separation evolution:

$$\frac{A_f}{A_i} = \left( \frac{M_{1i}}{M_{1f}} \right)^2 \left( \frac{M_{1f} + M_{2i}}{M_{1i} + M_{2i}} \right) \left( 1 - \gamma \frac{M_{1i} - M_{1f}}{M_{1i} + M_{2i}} \right)^2. \quad (8)$$

In any case and in either formalism, for surviving systems it is assumed that a CE phase is of such short duration (evidenced by the fact that it has never been observed with certainty) that the gainer is incapable of accreting any matter, resulting in  $\beta = 0$ .

It is possible for a donor star that has performed case A or B (either Br or Bc) RLOF to fill its Roche lobe again for a second time later in its evolution, as a helium star. This is known as case BB mass transfer (see De Greve & De Loore 1976; Delgado & Thomas 1981). Because the mass transfer rates involved are typically much lower than during the first RLOF, it is assumed that the non-degenerate gainer will accrete all of the matter lost during this episode, i.e.  $\beta = 1$ .

At a later point in the evolution, after the originally most massive star has become a WD, the originally least massive star will also fill its Roche lobe, initiating a mass transfer episode in the other direction. Because of the fact that the accreting star is a WD with a small surface, and because the mass ratio between the two stars is often very large, it is assumed that this will always lead to an unstable episode, resulting in a spiral-in. Therefore, it is modeled as a CE phase. One exception is when the combination of companion mass and orbital period identifies the system as a SD SN Ia progenitor (see next subsection).

## 2.2. Type Ia supernova progenitors

In this study, mainly the two most popular formation channels for SNe Ia are considered, the single degenerate (SD) and double degenerate (DD) scenario. Various others, including the so called core degenerate channel (Kashi & Soker 2011), various delayed detonation models (e.g. Hachisu et al. 2012), etc. have tentatively been included in our population synthesis code, but none of them has proven to be able to result in a notable number of SNe Ia at the right time (see Sect. 3). Interestingly, the progenitor parameter spaces of SD and DD events do not overlap, implying that it is possible that both formation channels are at work simultaneously.

### 2.2.1. Single degenerate scenario

For the SD scenario progenitors, we do not explicitly calculate the mass accretion on the WD ourselves, but we make use of the results of the groups that treated this scenario in detail. When in

a binary star consisting of a non-degenerate star and a WD, the former fills its Roche lobe, Hachisu et al. (1999, 2008) identified those zones (dependent on the WD mass) in the (companion mass, orbital period)-plane for which the mass transfer rate will fall within the narrow zone in which stable accretion up to the critical mass (assumed to be the Chandrasekhar mass of  $1.4 M_{\odot}$ ) is possible. There are two such zones: one for (late) MS companions, and one for RG companions, the latter requiring a larger orbital period. It should be noted that most population synthesis studies fail to reproduce a numerous amount of systems in the latter zone (see e.g. Han & Podsiadlowski 2004). This is suspicious, since systems of this nature (though not all necessarily SN Ia progenitors) are indeed quite abundantly observed, and known as the so called symbiotic stars (see e.g. Belczyński et al. 2000). The size and location in the  $(M_2, P)$ -plane of the zone with WD+MS progenitors is strongly dependent on the assumptions about the WD wind. Hachisu et al. (2008) propose the mass stripping effect, in which a strong wind from the WD blows away a significant amount of the matter lost by the non-degenerate star, thereby allowing some systems to avoid the CE phase they would otherwise have undergone. The strength of this wind is regulated by the parameter  $c_1$ , which determines the amount of stripped matter:

$$\frac{dM_{\text{strip}}}{dt} = c_1 \frac{dM_{\text{wind}}}{dt}. \quad (9)$$

The authors proposed a generic value of  $c_1 = 3$ , while it is stated that observations allow values anywhere between 0 (turning the effect off) and 10. One of the aims of the current paper will be to constrain this parameter further. As an illustration, a  $c_1$  of 3 about triples the area of the WD+MS progenitor zone compared to  $c_1 = 0$ . Finally, the efficiency of the SD scenario also critically depends on the metallicity, since in low metallicity systems, the WD wind will not be sufficiently strong to regulate the mass stream. Kobayashi et al. (1998) calculated the zones for  $Z=0.004$ , so that combination with the results of Hachisu et al. (1999, 2008) for  $Z=0.02$  allows to interpolate for any  $Z$ . In the population code, whenever a WD + non-degenerate system falls within such a SD SN Ia progenitor zone, it is assumed that this system will result in a SN Ia within a time that is negligible compared to the previous nuclear timescale of the stars.

### 2.2.2. Double degenerate scenario

Concerning the DD scenario, it is assumed that every merger of two WDs, together meeting or exceeding the Chandrasekhar limit of  $1.4 M_{\odot}$ , will result in a SN Ia at the time that GWR has reduced the distance between both to zero. It should be remarked that this spiral-in timescale is by no means negligible compared to the time needed to obtain a double WD. Because the exact physics of the explosion are as yet unclear and it is widely believed that the scenario only works for the merger of two C-O WDs, our computations are also performed with this additional restriction. Pursuant to recent speculation on the matter, we also investigate the influence on the population assuming sub-Chandrasekhar C-O WD mergers to result in SNe Ia.

It is of importance to repeat that there are two typical ways in which a double WD, eventually resulting in a DD SN Ia, can be formed. To obtain a double WD in an interacting binary<sup>1</sup> the primary and secondary need to fill their Roche lobes successively, resulting in two mass transfer phases. The first of these

<sup>1</sup> In a non-interacting binary, the orbital separation of the double WD will be much too large for it to merge within a Hubble time.

two phases can either be a stable RLOF event (either conservative or non-conservative) or result in an unstable CE evolution. As explained in Sect. 2.1, the second phase is assumed to result always in a CE phase, since the accretor is a WD. Detailed descriptions of either evolution channel as well as typical examples are given in M10. The conclusion is that double WDs having gone through two successive CE phases produce DD SNe Ia already after a few hundred Myr, while events having undergone a RLOF event have a delay time of up to several Gyr, but require the RLOF to be (quasi-)conservative to avoid merging of the components.

### 2.3. The Brussels galactic evolution model

The galactic code combines different output sets of the population code with a galaxy formation model to self-consistently calculate the star formation rate (SFR) and the subsequent chemical evolution of a galaxy. To provide sufficient room for interpolation, the chemical enrichment (including SNe Ia) by a starburst is included on the one hand for a population of single stars, on the other for a population of 100% binaries, and this for four different metallicities:  $Z=0$  (obtained by extrapolation), 0.0002, 0.002 and 0.02. It concerns a full set of yields as discussed by De Donder & Vanbeveren (2004), based on those of Woosley & Weaver (1995) but in particular, as motivated in the former paper, with the iron core-collapse yields divided by a factor of two. Combination with the current SFR, binary fraction and metallicity thus allows to calculate the current chemical abundances and SN Ia rate at any time. As was already found by De Donder & Vanbeveren (2004), one of the most important ways in which binaries significantly alter the chemical history of a galaxy compared to the computations with single stars only, is by the chemical enrichment (especially in iron) caused by SNe Ia. Therefore, it is critical that the rate of these events be an integral part of every chemical evolution model, which is physically sound and consistent with other ingredients, and not just “imported” from observations, let alone a free parameter.

Concerning the binary frequency, there are two possible assumptions: either this value is assumed to be constant in space and time, or it is treated as a function of metallicity. The latter assumption, a binary frequency that linearly increases with  $Z$ , does not produce any models that satisfactorily reproduce the chemical evolution of the solar neighborhood (as will be shown in Sect. 3). Therefore, a constant binary frequency is assumed, with a value of 70%. This reasonably high value is required in order to produce sufficient SNe Ia (which can obviously only occur in binaries) to attain the observed SN Ia rate and the necessary SN Ia-specific chemical (iron-)enrichment. This is consistent with the results of M10, where it was found that a very high binary frequency is also required (and not even sufficient) to explain the absolute number of SNe Ia observed in elliptical (starburst) galaxies.

Another important ingredient of any galactic evolution code is a galaxy formation model. This describes not only how the galaxy itself was formed, but more critically also provides a way to calculate the SFR as a function of time. The evolution of the SFR critically determines the chemical composition, SN Ia rate, etc. An often used galaxy formation model is the two-infall model by Chiappini et al. (1997). This model assumes that the Milky Way Galaxy was formed by two successive gas infall phases, the first forming the thick disk (including halo and

bulge), the second the thin disk. The gas infall rate in either phase is given by the following relation:

$$\frac{d\sigma_{g,inf}(t)}{dt} = Ae^{-t/\tau_1} + Be^{-(t-t_{max})/\tau_2}. \quad (10)$$

In principle, this equation obviously also depends on the distance to the galactic center, however since we only consider the solar neighborhood we are only concerned with applying it there.  $\tau_1$  and  $\tau_2$  are the mass accretion timescales for the halo and disk phase, which are taken as 2 Gyr and 7 Gyr (at the position of the Sun) respectively.  $t_{max}$  is the time of maximum accretion on the thin disk, and is equal to 1 Gyr. The values of the scaling parameters  $A$  and  $B$  are determined by the requirement of the galaxy formation model to reproduce the current observational constraints. The SFR is assumed to depend on both the gas surface density  $\sigma_g(t)$  and the total mass surface density  $\sigma(t)$ . Chiosi (1980) adapted the prescription of Talbot & Arnett (1975) to the infall model:

$$\Psi(t) = \nu \left( \frac{\sigma(t_{now})}{\sigma(t)} \right)^{k-1} \left( \frac{\sigma_g(t)}{\sigma(t_{now})} \right)^k \quad (11)$$

where  $\nu$  is the star formation efficiency in  $\text{Gyr}^{-1}$ . Both this parameter and  $k$  can be different during the first and second infall phase.  $\Psi(t)$  is set to 0 if  $\sigma_g(t)$  is below  $7 \text{ M}_\odot/\text{pc}^2$ . The favored model takes values of respectively 2 and  $1 \text{ Gyr}^{-1}$  for the efficiencies, and  $k = 1.5$  in both phases. It should be noted that the values of the parameters described here and used in this paper are taken from Matteucci et al. (2009) and differ from those in the original two-infall model by Chiappini et al. (1997) which were used in previous papers by the Brussels group. Notably, the ‘new’ values result in a SFR that is much less concentrated at early times, and instead is more flattened out.

A second possible galaxy formation model that is considered in this paper is simply a constant SFR. The onset of star formation is assumed to be delayed by 0.5 Gyr, which is the required time to allow the surface gas density to rise to  $7 \text{ M}_\odot/\text{pc}^2$ . After that, the SFR is constant with its value determined by the currently observed gas and star densities. This turns out to be about  $4 \text{ M}_\odot/\text{pc}^2\text{Gyr}$ , resulting in a total star formation roughly equal to the case of the two-infall model.

In both cases, the infalling primordial gas has a composition of  $X=0.76$ ,  $Y=0.24$  and  $Z=0$ .

Since a similar study by De Donder & Vanbeveren (2004), studies of the same kind have been performed by Greggio et al. (2008), Matteucci et al. (2009) (albeit both not with internally computed SN Ia DTDs, but with various adopted ones) and Kobayashi & Nakasato (2011) (albeit for the SD scenario only). The former three concluded that the best match between prediction and observation was found when both the SD and DD model were combined.

### 2.4. Observational galactic parameters

A critical prediction made by galactic evolution models is the abundance of various chemical elements. These are usually expressed logarithmically, relative to hydrogen (H), and normalized to the solar abundance. In this context, the most important abundance is that of the element iron (Fe). For the chemical yields of a single SN Ia event, those of the W7 model by Iwamoto et al. (1999) are assumed, both for SD and DD progenitors. Most importantly, this includes a yield of  $0.626 \text{ M}_\odot$  Fe per SN Ia.

The age-metallicity relation (AMR) is the evolution of  $[\text{Fe}/\text{H}] (= \log(\text{Fe}/\text{H}) - \log(\text{Fe}/\text{H})_\odot)$  as a function of time. Stars that are formed at a certain time are obviously assumed to contain the metallicity of that instant. Therefore, if these stars are still observable today, and their age can be determined, they provide a way to reconstruct the chemical history of the Galaxy. Stars that are very suited for this purpose are the G-type dwarfs ( $0.80M_\odot \leq M \leq 1.05M_\odot$ ), since they have an extremely long lifetime of up to the age of the Galaxy itself. Therefore, the metallicity distribution of these local G-type dwarfs, i.e. the relative number of observed G-dwarfs with respective  $[\text{Fe}/\text{H}]$ , is indicative of the entire chemical history of the solar neighborhood. Since the DTDs of SD and DD SN Ia progenitors are markedly different, this chemical history should be critically influenced by which scenario is at work.

The observational G-dwarf metallicity distributions that will be used for comparison in this paper are those by Holmberg et al. (2007). Two distributions are derived in this paper, one for a spherical solar neighborhood and one for a cylindrical one. Since in our galactic code the solar neighborhood is defined as a cylindrical region of 1 kpc around the Sun, mainly the latter will be used. It should be noted that a more recent analysis of the Geneva-Copenhagen survey data by Casagrande et al. (2011) results in a slightly different G-dwarf metallicity distribution, which has the same morphological shape but peaks at a slightly higher value of  $[\text{Fe}/\text{H}]$ . As the difference ( $\sim 0.1$  dex) is not too large, and the Holmberg et al. (2007) distribution provides the advantage of having been explicitly calculated also for a cylindrical solar neighborhood, the latter will be used for comparison. Additionally, if theoretical models are ruled out by being unable to produce enough Fe, these conclusions will not be affected if an even higher  $[\text{Fe}/\text{H}]$  must be matched.

While the G-dwarf metallicity distribution seems quite robust (those already mentioned are quite similar to the ones by Lee et al. (2011), and also numerous others found in the literature over the past decade), the same is not true for the AMR. As will be elaborated on in Sect. 3.2, the recent literature contains a wide variety of such observed relations, depending on the method of their construction. Some of these AMRs show a rising trend in  $[\text{Fe}/\text{H}]$  as a function of time, while others do not. Also the width of the AMR (i.e. the extent of scatter in  $[\text{Fe}/\text{H}]$  at a given age) and its possible origins is a matter of debate. For this reason, our comparison between prediction and observation will focus mainly on the G-dwarf metallicity distributions themselves, and less on the AMR.

A chemical evolution model also needs to explain the evolution of the abundance of other chemical elements, in particular  $[\text{O}/\text{Fe}]$  and  $[\text{C}/\text{Fe}]$  vs.  $[\text{Fe}/\text{H}]$ . Especially  $[\text{C}/\text{Fe}]$  is influenced by binary effects other than SNe Ia.

#### 2.4.1. Comparison method

The current age of the Galaxy is taken to be 13.2 Gyr, the time after which the theoretically obtained star and gas surface densities are compared to the currently observed ones. The latter are taken from Calura et al. (2010) and references therein, yielding  $37.5 \pm 10 M_\odot \text{pc}^{-2}$  for the stellar surface density and  $10.5 \pm 3.5 M_\odot \text{pc}^{-2}$  for the gas surface density. Other parameter-sensitive output that can be compared to current values are a SFR of  $3.5 \pm 1.5 M_\odot \text{pc}^{-2} \text{Gyr}^{-1}$  (according to the same source's analysis of Rana 1991) and a local SN Ia rate of  $0.003 \pm 0.002 \text{pc}^{-2} \text{Gyr}^{-1}$  (according to the analysis of Cappellaro 1996). The latter corresponds to  $3 \pm 2$  SNe Ia per millennium in the Milky Way Galaxy. Only when these values are reproduced to within the observa-

tional uncertainty is a model considered as possibly valid. The final distributions that then need to be checked, the actual goal of the study, are the C and O histories and, most importantly, the G-dwarf metallicity distribution.

Using the same Kroupa et al. (1993) IMF as the population code, the galactic code calculates from the SFR how many G-dwarfs are being born at any given time. These are obviously assumed to contain the metallicity that is prevalent at the time of their birth. Taking into account the mass-dependent lifetime of each G-dwarf, it is then calculated which fraction of those born at each timestep is still observable today. The  $[\text{Fe}/\text{H}]$ -distribution of these remaining stars is then plotted in a histogram with bin size 0.1 dex, ready to be compared to observations. Theoretically, every star born at the same time thus has the same Fe-content. As mentioned before, however, observations indicate that this may not be the case in reality (Ramírez et al. 2007; Holmberg et al. 2007; Casagrande et al. 2011). It may thus prove to be necessary to supplement the theoretically obtained  $[\text{Fe}/\text{H}]$  at each moment with a random (positive or negative) deviation, e.g. distributed following a certain standard deviation. A possible reason for this “intrinsic scatter” in the AMR is the radial migration of stars over large galactocentric distances (Roškar et al. 2008). The possible implications of this open question for the results of this study will be discussed in Sect. 3.2.

It should be noted that the early  $[\text{C}/\text{Fe}]$  and  $[\text{O}/\text{Fe}]$  vs.  $[\text{Fe}/\text{H}]$  evolution is extremely sensitive to the assumptions about direct black hole formation, i.e. whether and how much SN ejecta are expelled by massive stars prior to collapse, and what the lower mass limit for this process is. The current calculations have been performed under the assumption that stars above  $40 M_\odot$  will form a black hole with the hypernova yields of Nakamura et al. (2001), the total ejected mass so chosen that  $4 M_\odot$  of O is expelled per event (see De Donder & Vanbeveren 2003). Other choices do not more than marginally influence the C and O histories at  $[\text{Fe}/\text{H}] > -1.5$ , nor the G-dwarf metallicity distribution. As a remark, the solar reference values used in the determination of  $[\text{Fe}/\text{H}]$ ,  $[\text{C}/\text{Fe}]$  and  $[\text{O}/\text{Fe}]$  are the actual solar abundances, not those predicted by the model. Choosing the latter would obviously force the curves through the origin.

### 3. Results and discussion

Anticipating the results in this section, we find that reproducing the observed DTD is a necessary but not sufficient condition for a certain combination of assumptions to satisfactorily reproduce the observed G-dwarf metallicity distribution. Therefore, the first test will again focus on those DTDs. Only when the DTD is in agreement with the observed ones can there be hope of reproducing the observed G-dwarf metallicity distribution in a second step. A good DTD is however no guarantee for success, not only because of galactic evolutionary considerations, but also because of the limited timeframe during which the theoretical DTD can be compared with observation: at early times no observational test for the DTD is available, while this part obviously also contributes to the galactic chemical evolution. Hence there will be a considerable difference between the G-dwarf metallicity distributions obtained for the following fictional DTDs: (a) one matching the observational data points and with a late onset just in time to match the earliest such point (at 175 Myr); (b) one matching the observational data points but with a very early onset of 50 Myr; (c) one matching the observational data points and with an intermediate onset of 85 Myr

(resulting in the best match for the G-dwarf metallicity distribution).

Additionally, whether a non-fictional model with satisfactory DTD will also reproduce the observed G-dwarf metallicity distribution critically depends on the Z-sensitivity of the model. The DD channel is relatively independent of metallicity, its efficiency even increasing a bit with lower Z. However, the number of events produced by the SD channel is decimated when Z is lowered from 0.02 to 0.002, and reduces to zero for even lower Z. This is of course a result of the WD wind no longer being able to stabilize the mass stream (see Sect. 2.2.1). This means that a model which solely relies on the SD channel to produce SNe Ia with short delays, will only be able to provide these events (and their Fe enrichment) after the metallicity has already been enhanced. Hence, the early evolution of the galaxy will be characterized by Fe-deficiency.

### 3.1. Delay time and G-dwarf metallicity distribution

In this subsection we will first establish our standard model of parameters and other assumptions, as also used in M10. It will be shown that this model, with neither progenitor scenario nor with both combined, is satisfactory, even with the suggestions for improvement made in that paper. Thus, we will investigate what changes in the assumptions would be required to mitigate the discrepancy between prediction and observation. Subsequently, the following will be studied:

- the influence of angular momentum assumptions ( $\alpha$  vs.  $\gamma$ -scenario for CE, values of parameters, modeling of angular momentum loss)
- whether inclusion of any non-traditional SN Ia progenitor scenarios can significantly change the picture
- the influence of uncertainties intrinsic to the radiational progenitor scenarios (what is the best value for  $c_1$  in SD systems, are DD SNe Ia restricted to C-O WD mergers, do sub-Chandrasekhar C-O WD mergers also explode?)
- all along, also the influence of galactic evolutionary parameters and assumptions (e.g. galaxy formation model, binary frequency type and value) will be studied.

The DTDs obtained with the population code for a single starburst consisting of 100% binaries are shown in Fig. 1. Represented are the SD DTD for  $\beta_{\max} = 1$  and  $c_1 = 3$ , as well as the DD DTDs for  $\beta_{\max} = 1$ , respectively 0. Superimposed are the observational DTDs of Totani et al. (2008) (including one data point by Mannucci et al. 2005) and Maoz et al. (2012). The SD DTD for  $\beta_{\max} = 0$  barely differs from the one shown. Other assumptions are  $Z=0.02$ ,  $\alpha\lambda = 1$  and a flat mass ratio distribution. As already concluded by M10, independent of the latter choices, the SD DTD drops away too fast and too soon to keep matching the observations after a few Gyr, even with values for  $c_1$  up to 10. For  $\beta_{\max} = 1$  the DD distribution matches the observations in morphological shape, but lies a factor 2-3 too low in absolute value at the 11 Gyr point. The drastic decrease in the DD DTD for  $\beta_{\max} = 0$  means two things: firstly, the events which disappear in the latter case (about 80% of all DD SNe Ia) have all gone through a stable RLOF event and thus not two CEs; secondly, in order to be able to reproduce the morphological shape of the observations,  $\beta_{\max}$  needs to be close to 1, i.e.  $\geq 0.9$ . Concerning the SD events, as already touched upon in Sect. 2.2.1, we also find very few WD+RG progenitors, most events occurring in WD+MS systems. Also shown in the figure is the combination of both SD and DD, albeit with  $c_1 = 1$  and

assuming a 10% increase in convective core mass due to rotation (as proposed by M10), the latter mainly enhancing the DD channel. This combination matches the observed DTDs both in shape and number, but as will be seen later this does not automatically mean that inserting this DTD in the galactic model will yield a satisfactory galactic chemical evolution outcome.

Fig. 2 shows the G-dwarf metallicity distribution obtained with only the SD and DD channel respectively. The SD rates have been calculated with  $c_1 = 3$ , a moderately high value which results in rates only marginally smaller than if the maximum value of  $c_1 = 10$  would be chosen. While the DD DTD is the only one still compatible with the observations in morphological shape, it is obvious that the G-dwarf metallicity distribution does not correspond to observations. The same is true to an even more dramatic extent for the SD channel. In none of the performed simulations, with none of the stellar or galactic evolutionary parameter choices, we obtain a situation in which either scenario alone succeeds in even marginally reproducing the observed G-dwarf metallicity distribution.

As does Fig. 1, M10 showed that when a 10% increase in convective core mass is assumed, the combined SD + DD model matches the observational DTDs well. However, it is obvious from Fig. 2 that this is not true for the corresponding G-dwarf metallicity distribution. This shows that the distribution peaks at too low [Fe/H] values, indicating that not enough Fe is formed early on in the galactic evolution. This conclusion stands independent of the chosen value for  $c_1$ . The reason is that the early part of the DTD, prior to the first observational test, does not provide enough Fe pollution soon after the starburst. These early events are caused through the SD channel (which is not much affected by the convective core mass increase and does not work for low Z anyway), as well as through WD mergers already massive enough without the increase. As will be shown later, if early events would also increase by a factor of 2-3, the G-dwarf metallicity distribution would match observations. Obviously, the distribution for the combined SD + DD model but without convective core mass increase (also shown in Fig. 2) results in an even poorer match with observations.

As an academic exercise, Fig. 3 shows the G-dwarf metallicity distribution which is obtained when the standard model SD and DD channels (from Fig. 1) are combined, but multiplied by a factor of 2.5 over the entire time range<sup>2</sup>. In that case, the DTD perfectly matches the observations. When the standard two-infall model is used, this results in a G-dwarf metallicity distribution that peaks in the correct location, but with much less spread than the observations. On the other hand, when a constant SFR is assumed, the predicted G-dwarf metallicity distribution shows a good match with the observed one. As a side note, it is remarkable that the one obtained with the two-infall model shows a better resemblance with the observational distribution obtained for a spherical solar neighborhood as is used for comparison by Kobayashi & Nakasato (2011).

The DTDs and the resulting G-dwarf metallicity distribution were also calculated using the  $\gamma$ -scenario for CE evolution in the first mass transfer phase. The results are shown in Fig. 4 and 5 respectively. The same figures also show the results obtained with the  $\alpha$ -scenario for CE evolution, but with the  $\alpha\lambda$  parameter not set to the same fixed value for all stars but instead calculated separately for each system according to the results of Dewi & Tauris (2000), resulting in values for this parameter

<sup>2</sup> To allow for straightforward comparison, the same factor of 2.5 will be used in several subsequent models that otherwise underestimate the observed Fe-abundances.



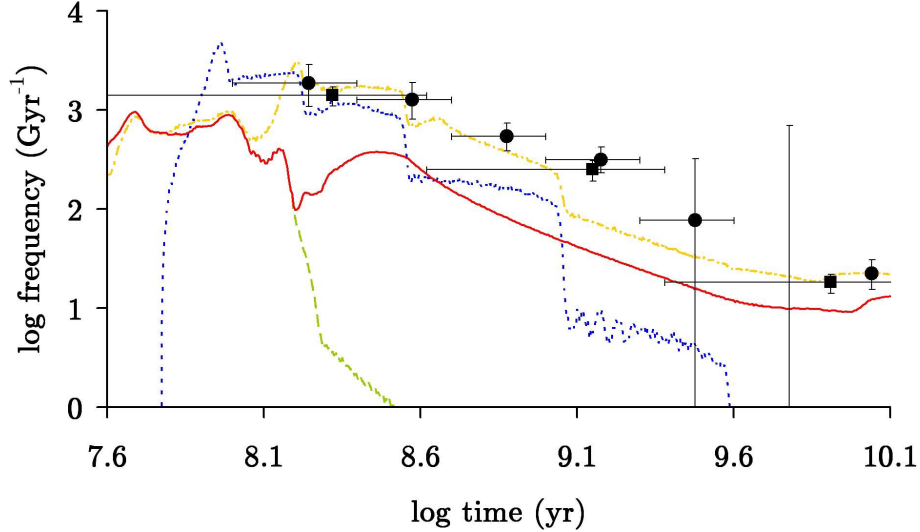


**Fig. 1.** DTDs obtained with the DD scenario for  $\beta_{\max} = 1$  (solid) and  $\beta_{\max} = 0$  (dashed), as well as with the SD scenario for  $\beta_{\max} = 1$  and  $c_1 = 3$  (dotted). Combined SD + DD model DTD with  $\beta_{\max} = 1$  and  $c_1 = 1$ , but with a convective core mass increase of 10% (dashed-dotted). Observational data points by Totani et al. (2008) (circles) and Maoz et al. (2012) (squares).

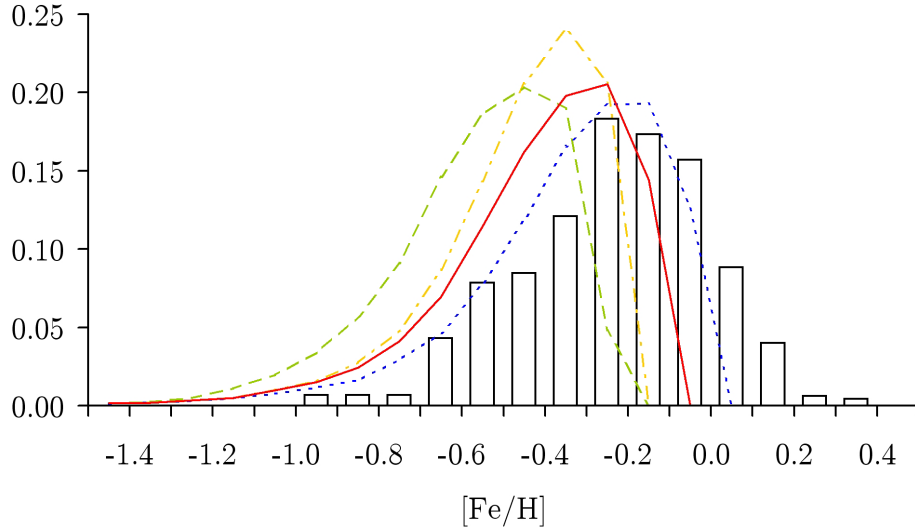


**Fig. 2.** G-dwarf metallicity distributions obtained with the combined SD (with  $c_1 = 3$ ) + DD model either without (solid) or with (dotted) 10% convective core mass increase, as well as for the SD (with  $c_1 = 3$ , dashed) respectively DD (dashed-dotted) scenario alone. Observational data for a cylindrical solar neighborhood (white histogram) by Holmberg et al. (2007).

much smaller than one, on average  $\alpha\lambda \approx 0.25$ . It can be summarized that for both alternative CE treatments the conclusions are similar as for the standard  $\alpha$ -scenario: in order to reproduce the observed G-dwarf metallicity distribution, the absolute number of SN Ia events needs to be multiplied by 2.5. This then also results in a DTD matching the observed one. Only when using the  $\alpha\lambda$ -values by Dewi & Tauris (2000) does this multiplication result in a slight Fe-overabundance, indicating that a lower multiplication factor is needed there for the best match. Also notable is that when using the  $\gamma$ -scenario, the morphological shape of the G-dwarf metallicity distribution is acceptable for both the two-infall model and the constant SFR.

Use of the specific gainer orbital angular momentum loss assumption instead of the  $L_2$  one (see Sect. 2.1) results for  $\beta_{\max} = 1$  in SD and DD SN Ia rates changing by not more than some 10%, nor is the morphological shape of the DTD severely altered. The same is thus also true for the resulting G-dwarf metallicity distributions and the conclusions from those. One possibly important

difference is that with this angular momentum loss assumption, in the case of  $\beta_{\max} = 0$ , the distributions are not greatly influenced compared to  $\beta_{\max} = 1$ , owing to the very limited angular momentum loss. Thus, much lower values of  $\beta$  than with the  $L_2$  assumption still yield DTDs compatible in morphological shape with the observations.

When the standard SD + DD model is considered, but with DD SNe Ia restricted to the merger of two C-O WDs (and still exceeding the Chandrasekhar limit), the total number of SNe Ia goes down by some 20%, but this does not compromise the morphological shape of the DTD. The corresponding G-dwarf metallicity distribution, again for the DTD multiplied by a factor of 2.5, is also shown in Fig. 5. It demonstrates that to obtain a satisfactory distribution, the multiplication factor then merely has to be increased slightly.

One of the non-standard SN Ia formation scenarios that has been tested is the core-degenerate (CD) channel (Kashi & Soker 2011). For this, it is assumed that the merger of a WD



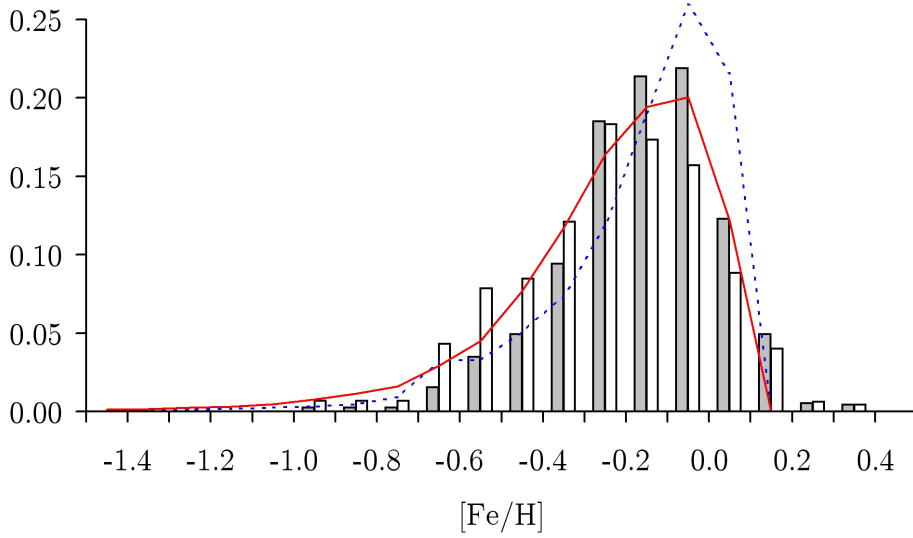


**Fig. 3.** G-dwarf metallicity distributions obtained with the combined SD (with  $c_1 = 1$ ) + DD model, with SN Ia rates multiplied by a factor of 2.5, for a constant SFR (solid) and for the two-infall model (dotted). Observational data for a spherical (gray histogram) and cylindrical (white histogram) solar neighborhood by Holmberg et al. (2007).

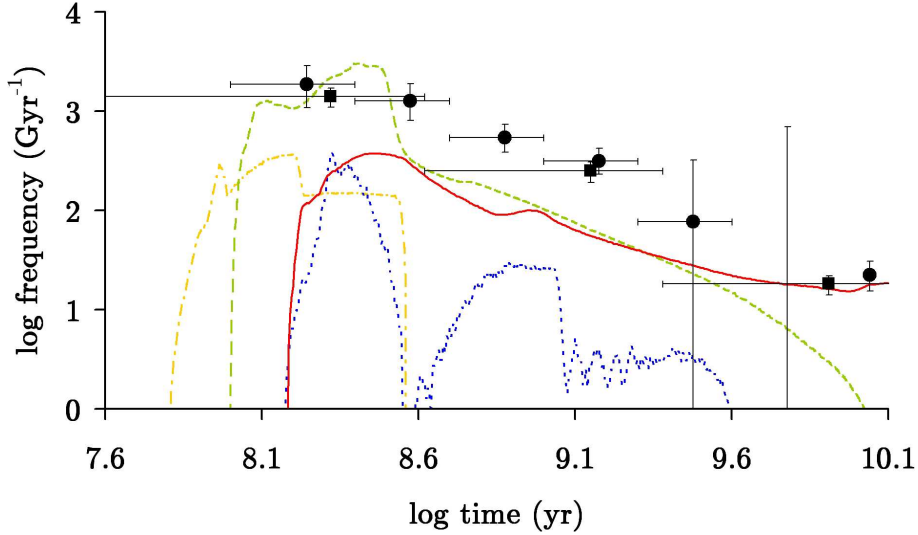


**Fig. 4.** DTDs obtained with the  $\gamma$ -scenario for CE-evolution through the DD (solid) and SD (dotted) channel. DTDs obtained with the  $\alpha$ -scenario, using the parameter values determined by Dewi & Tauris (2000), through the DD (dashed) and SD (dashed-dotted) channel. Observational data points by Totani et al. (2008) (circles) and Maoz et al. (2012) (squares).

with the core of a non-degenerate star, together exceeding the Chandrasekhar mass, will result in a SN Ia. This merger can happen at any time between the formation of the first and second WD, but most likely during a CE phase. According to Ilkov & Soker (2012a), the SN Ia does not necessarily take place at the time of merger: if they have a rapid rate of rigid rotation, the explosion of merger products with a mass below  $1.48 M_{\odot}$  can be delayed by a significant time (up to 10 Gyr), until magnetic braking has provided enough downspin. This can not only deliver the events with long delay time, but can also explain the absence of H in the spectrum of the explosion. It should also be noted that the CD channel is relatively independent of the  $\alpha\lambda$  parameter of CE evolution. If this product is set to 0.1 instead of 1, the CD rate changes by only -15%, compared to -95% and +80% for SD and DD respectively. Also the corresponding change in morphological shape of the distribution is much smaller than for those two. However, as was already

shown by M10 (without making reference to SNe Ia) the number of WD + non-degenerate mergers is extremely large immediately after starburst, but then drops very fast (with the number of such events sharply falling by several orders of magnitude after 0.3 Gyr). Although the total number of these potential CD events matches the total number of SNe Ia quite well (as noted by Ilkov & Soker 2012b), we thus find that the number of early events ( $< 0.3$  Gyr) lies much too high to match the observed DTD, while the number of late events ( $> 0.4$  Gyr) lies much too low. The mentioned delay between merger and explosion does not solve this problem, as it can only apply to systems with a total mass  $< 1.48 M_{\odot}$ , which represent only 10% of the total. Also the G-dwarf metallicity distribution obtained under the CD assumption is unable to match the observed one: owing to the extremely high number of events (up to  $> 10^4 \text{ Gyr}^{-1}$ ) at early times, it results in a strong Fe-overproduction regardless of other

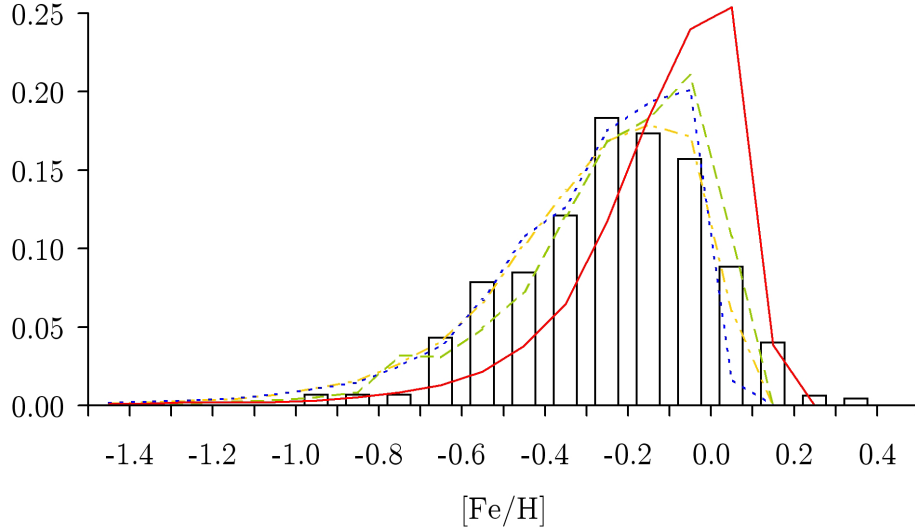


**Fig. 5.** G-dwarf metallicity distributions obtained with the combined SD (with  $c_1 = 3$ ) + DD model, all with SN Ia rates multiplied by a factor of 2.5, for the  $\alpha$ -formalism with parameter values by Dewi & Tauris (2000) (solid), for the  $\gamma$ -formalism and either a constant SFR (dotted) or the two-infall model (dashed), as well as for the standard  $\alpha$ -formalism but with only super-Chandra CO WD mergers resulting in DD SNe Ia (dashed-dotted). Observational data for a cylindrical solar neighborhood (white histogram) by Holmberg et al. (2007).

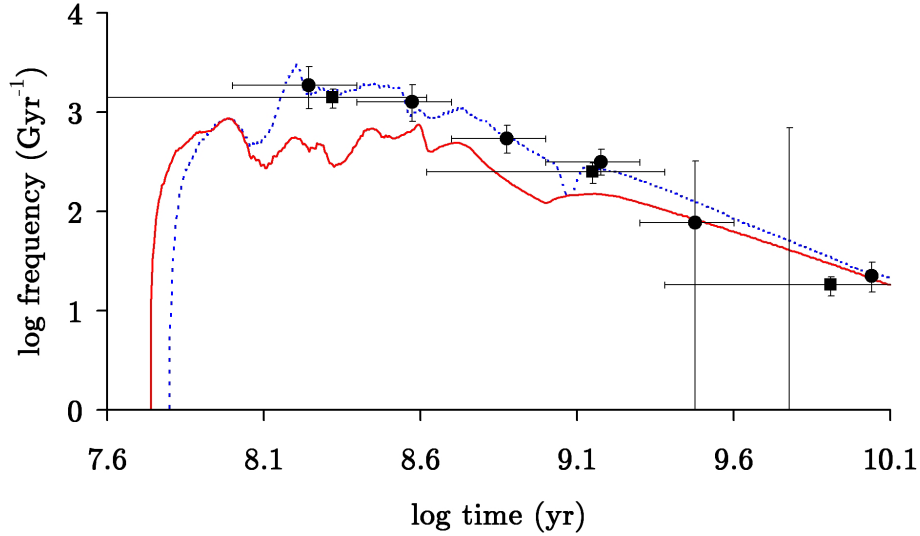


**Fig. 6.** DTD obtained with the assumption that all double C-O WD mergers result in SNe Ia, through the DD (solid) channel. Combined SD (with  $c_1 = 1$ ) + DD model DTD under the same assumption, but with a convective core mass increase of 10% (dotted). Observational data points by Totani et al. (2008) (circles) and Maoz et al. (2012) (squares).

assumptions. These conclusions also stand under the additional restriction that the WD involved must be of the C-O type.

For the same reason, the delayed detonation SD model proposed by Hachisu et al. (2012) is unable to provide a significant increase in SNe Ia with long delay in our simulations. This scenario assumes that rotating WDs can accrete matter until highly exceeding the Chandrasekhar limit, not exploding until the star has spun down. However, only for the small minority of rigidly rotating WDs with a mass below  $1.5 M_{\odot}$  can this cause a significant delay.

Recently there has been much speculation about the possibility of sub-Chandrasekhar C-O WD mergers exploding as SNe Ia (see e.g. Badenes & Maoz 2012). Fig. 6 shows the DD DTD obtained under the assumption that all C-O WD mergers, regardless of their total mass, indeed result in such an event. This DTD (in combination with the SD channel from Fig. 1) shows a very

good agreement with the observational ones. However, as Fig. 7 shows, the obtained G-dwarf metallicity distribution shows not enough Fe enrichment, even though the discrepancy is not too large. The reason for this is again that at the very start of the DTD, before any comparison with observation is available, the SN Ia rate is low, especially for  $Z < 0.02$  (DTDs not shown). However, these very early events ( $< 0.1$  Gyr) seem to be required in order to cause enough Fe pollution at very low  $Z$  (and thus  $[\text{Fe}/\text{H}]$ ). Of course, this Fe might also have another source than SNe Ia. A simulation was run including the yields of very massive stars ( $140 M_{\odot} < M < 260 M_{\odot}$ ) at  $Z < 10^{-5}$  as computed by Heger & Woosley (2002), which liberate up to  $40 M_{\odot}$  of Fe each (see also Vanbeveren & De Donder 2006). Because the duration of this low metallicity phase is so short, the Fe produced during this era only greatly influences the chemical evolution at that time itself, and does not leave a lasting legacy once other

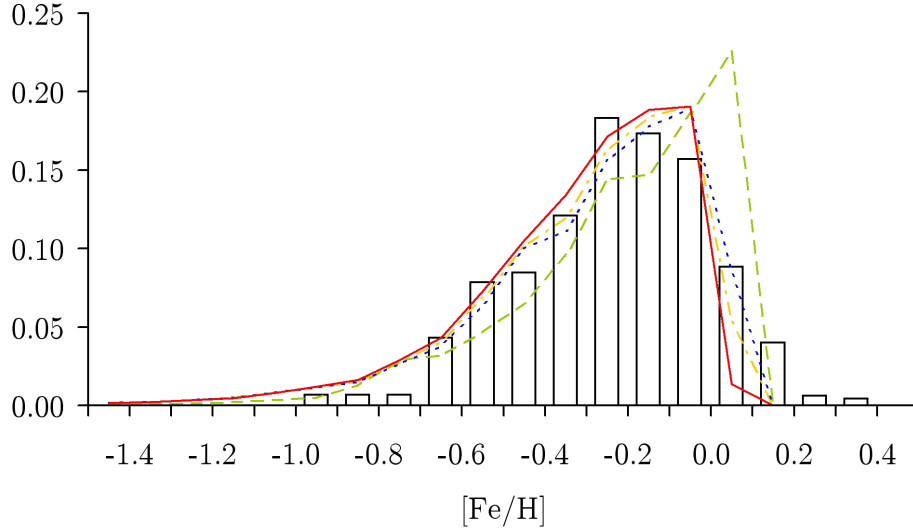


**Fig. 7.** G-dwarf metallicity distributions obtained with the combined SD + DD model, with  $c_1 = 3$  under the assumption that all double C-O WD mergers result in SNe Ia (solid), with  $c_1 = 1$  and the same assumption but for a convective core mass increase of 10% for either a constant SFR (dotted) or the two-infall model (dashed), as well as for a constant SFR but with SN Ia yields scaled to their total explosion mass if  $< 1.4 M_{\odot}$  (dashed-dotted). Observational data for a cylindrical solar neighborhood (white histogram) by Holmberg et al. (2007).

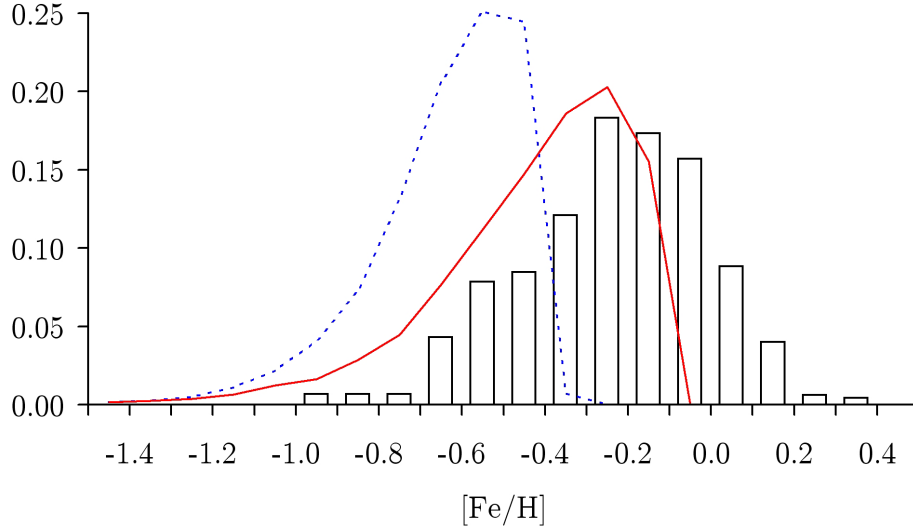


**Fig. 8.** G-dwarf metallicity distributions obtained with the combined SD (with  $c_1 = 1$ ) + DD model, with all double C-O WD mergers resulting in SNe Ia and a convective core mass increase of 10%, for a constant binary frequency of 35% (solid) and for a binary frequency increasing linearly with  $Z$  (dotted). Observational data for a cylindrical solar neighborhood (white histogram) by Holmberg et al. (2007).

sources of Fe (i.e. mainly the SNe Ia) turn on and soon drown it out. The origin of this early Fe thus remains unclear. Wang et al. (2009) propose a He-star channel which they claim leads to very early SNe Ia through the SD channel. When introduced into our population code however, this channel seems to produce only relatively late SNe Ia, and not many compared to the other channels. This seems logical, since in the SD channel one always needs the secondary to fill its Roche lobe towards the WD. As the maximum allowed secondary mass for this mass transfer to be stable is around  $3 M_{\odot}$ , it is obvious that this can take a while. One hypothetical solution to the situation is when one does not restrict the DD SN Ia explosions to C-O WDs. If, in addition to assuming that all C-O WD mergers explode (regardless of total mass), one also assumes that all super-Chandrasekhar mergers explode (regardless of composition), then the early-time events

(starting as early as 20 Myr) are provided by DD mergers where the more massive star is an ONeMg WD. Without compromising the shape and number of the DTD at times for which observations are available, the obtained G-dwarf metallicity distribution then shows an excellent match with the observations.

A much less artificial model, that also reproduces the observed G-dwarf metallicity distribution, is when the assumption about all C-O WD mergers exploding as SNe Ia is combined with the assumption about the 10% convective core mass increase. The then obtained DTD is also shown in Fig. 6 and perfectly matches the observations, without multiplication factor. The same is true for the corresponding G-dwarf metallicity distribution shown in Fig. 7. This figure shows three different distributions obtained under these assumptions. Firstly for the flat SFR vs. the two-infall model, both for  $c_1 = 1$ . This is the

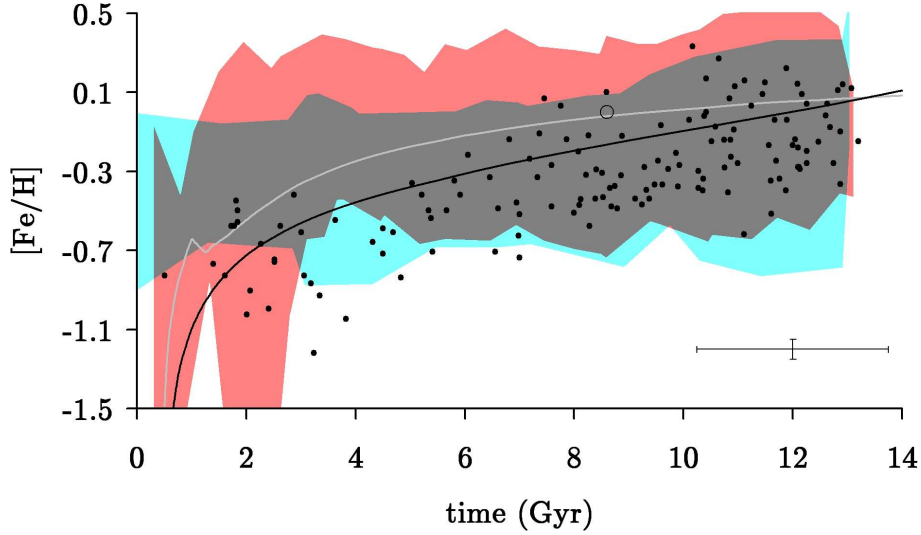


**Fig. 9.** AMR with the combined SD (with  $c_1 = 1$ ) + DD model, with all double C-O WD mergers resulting in SNe Ia and a convective core mass increase of 10%, for a constant SFR (black) and for the two-infall model (gray). Observational data points by Ramírez et al. (2007) (dots) and for the Sun (open circle), as well as zones (shaded) in which the data points by Holmberg et al. (2007) (lower) and Casagrande et al. (2011) (upper) lie, but see text for important note on their representativeness. At the lower right, the typical observational error bar for center of the plot (increasing towards the left) is shown.

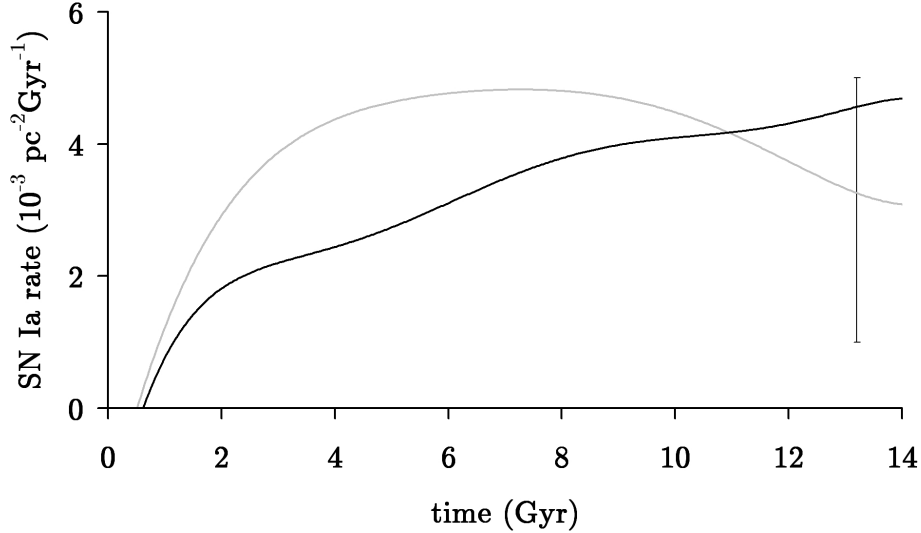


**Fig. 10.** SN Ia rate with the combined SD (with  $c_1 = 1$ ) + DD model, with all double C-O WD mergers resulting in SNe Ia and a convective core mass increase of 10%, for a constant SFR (black) and for the two-infall model (gray). Currently observed rate is indicated by error bar.

only model in which for a flat SFR stellar surface density, gas surface density and current SN Ia rate are within observational constraints at the same time. The model with  $c_1 = 3$  results in a slightly too high SN Ia rate (the same was true in the case of the combined SD + DD model multiplied by a factor of 2.5). The third distribution shown is also for a flat SFR, but with all DD SN Ia yields scaled to their total explosion mass (if below  $1.4 M_\odot$ ), i.e. taking into account the fact that a sub-Chandrasekhar DD SN Ia may well produce less Fe (and other yields) than a Chandrasekhar mass one. The figure shows however that this open question does not critically affect the metallicity distribution. Figure 7 shows a slight Fe-overproduction when using the SFR from the two-infall model. In that case, the assumption that all C-O WD mergers result in DD SNe Ia yields a better G-dwarf metallicity distribution without the additional assumption of a 10% convective core mass increase than with it. However, it

then only concerns the location of the peak of the distribution, its morphological shape is still reproduced better with the flat SFR.

Even in the case of the best model, the predicted G-dwarf metallicity distribution shows too little (i.e. no) stars with very high metallicity, and too many with very low metallicity. This is the case for all reasonably simple theoretical galactic chemical evolution models, and is long known as the G-dwarf problem. A possible way to mitigate the situation is by assuming that stars are not necessarily observed at the location of their birth (and for which their  $[\text{Fe}/\text{H}]$  is thus representative). Such a migration scenario (Roškar et al. 2008) allows to explain the observational presence of stars with higher metallicity than can be produced locally according to the model. Additionally, it allows to reproduce to a certain extent the intrinsic scatter in the AMR that is observed (i.e. the fact that not all stars born at the same time have the same  $[\text{Fe}/\text{H}]$  in reality, see also next subsection).

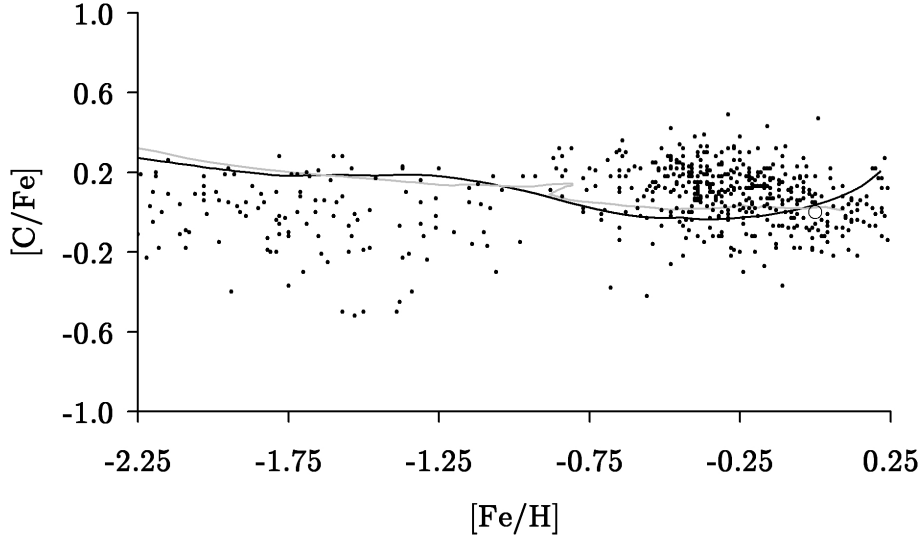


**Fig. 11.**  $[C/Fe]$  vs.  $[Fe/H]$  with the combined SD (with  $c_1 = 1$ ) + DD model, with all double C-O WD mergers resulting in SNe Ia and a convective core mass increase of 10%, for a constant SFR (black) and for the two-infall model (gray). Observational data by Chiappini et al. (2003), Reddy et al. (2003), Bensby & Feltzing (2006) and Fabbian et al. (2009) (dots) and for the Sun (open circle).

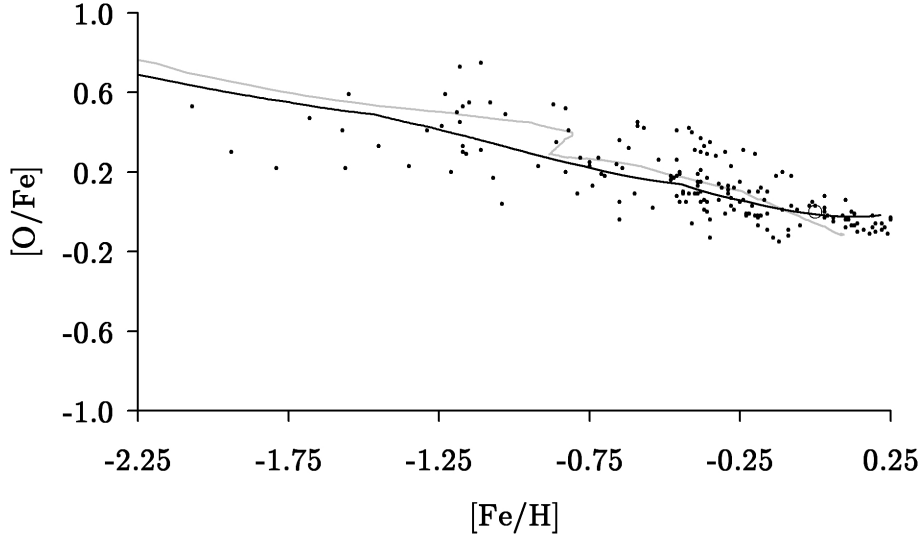


**Fig. 12.**  $[O/Fe]$  vs.  $[Fe/H]$  with the combined SD (with  $c_1 = 1$ ) + DD model, with all double C-O WD mergers resulting in SNe Ia and a convective core mass increase of 10%, for a constant SFR (black) and for the two-infall model (gray). Observational data by Gratton et al. (2003), Reddy et al. (2003) and Calura et al. (2010) (dots) and for the Sun (open circle).

As an illustration of the previously claimed requirement to have a high and constant binary frequency, Fig. 8 shows the same best model but for a binary frequency of 35% (half the standard value), respectively one varying linearly with  $Z$ . It is obvious that the G-dwarf metallicity distribution in both cases shows a very strong underproduction of Fe.

### 3.2. Other galactic evolutionary constraints

Figure 9 shows the AMR for the model which best approximates the observed G-dwarf metallicity distribution, i.e. the SD (with  $c_1 = 1$ ) + DD model but with all C-O WD mergers exploding as SN Ia and a convective core mass increase of 10%. This is done both for a constant SFR and for the SFR following from the two-infall model. It should be noted that distributions for other (reasonably) satisfactory models, such as the same model without

the core mass increase or the standard SD + DD model with SN Ia rates (artificially) enhanced by a factor of 2.5, look very similar. When the predicted AMR is compared to the observational ones obtained by Holmberg et al. (2007) and Casagrande et al. (2011), this is not very instructive. The latter namely suggest an AMR that is almost flat, but has a very significant and intrinsic scatter. As a result of the latter, all theoretical models produced in this study lie within the observationally populated zone, but none of them is able to reproduce an AMR with this general (lack of) shape. This is because the infalling pristine gas is unable to fully compensate for the large Fe-enrichment caused by SNe Ia. If the Holmberg et al. (2007) or Casagrande et al. (2011) AMR is indeed representative for the solar neighborhood as well as intrinsic (i.e. not caused by contamination effects due to dynamics), and thus the one to be reproduced, this presents a serious problem for theoretical predictions. As already mentioned in the

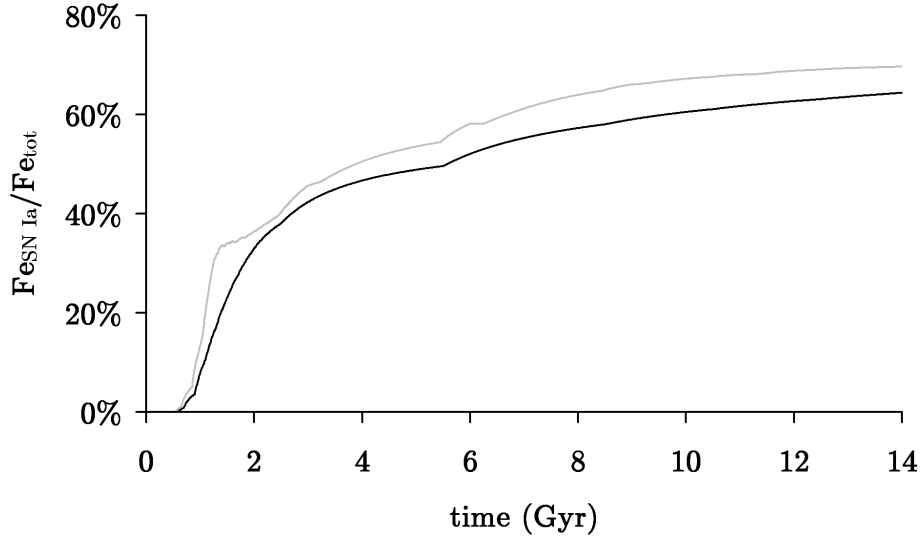


**Fig. 13.** Fraction of all Fe produced by SNe Ia with the combined SD (with  $c_1 = 1$ ) + DD model, with all double C-O WD mergers resulting in SNe Ia and a convective core mass increase of 10%, for a constant SFR (black) and for the two-infall model (gray).

context of the G-dwarf distribution, almost no theoretical chemical evolution models are able to produce an AMR that is flat throughout most of the Galaxy’s history, although again the radial migration assumption may help in this respect. However, an alternative AMR was derived by Ramírez et al. (2007) under different conditions on the star selection and especially the age uncertainty, as well as different stellar parameter zero points (especially temperature, leading to different ages). This observational AMR does indeed show a rise in function of time, as is predicted by theoretical evolution models. However, it is likely that this sample consisting of stars suitable for high-resolution high S/N spectral analysis is not representative for the solar neighborhood, as it is based on a collection of spectroscopic data for a very limited number of stars, selected in a non-random fashion, but poorly constrained nonetheless (I. Ramírez, personal communication, 2012). Nevertheless, this AMR is also shown in Fig. 9. Whether or not the Holmberg et al. (2007) or Casagrande et al. (2011) AMR are indeed representative for the solar neighborhood additionally depends on the validity of the used stellar isochrones. For completeness, it should also be noted that if one were to construct a G-dwarf metallicity distribution from the stars selected by Ramírez et al. (2007) for the construction of their AMR, this G-dwarf metallicity distribution would be extremely more spread out than the one by Holmberg et al. (2007) or Casagrande et al. (2011). While such distribution would be questionable due to the mentioned non-representative nature of the dataset, it is of interest to note that to retrieve such a spreaded G-dwarf metallicity distribution in our predictions, the intrinsic scatter added to the time-dependent  $[\text{Fe}/\text{H}]$  must be taken very large, to the extent where it would correspond to the entire scatter observed in the AMR.

The evolution of the SN Ia rate as a function of time is shown in Fig. 10, with the currently observed rate indicated. It shows an acceptable level of agreement with observation for either model, although it should be remembered from Fig. 7 that only for the flat SFR a good agreement in morphological shape was found for the G-dwarf metallicity distribution.

Figures 11 and 12 show the C and O abundance variation obtained with the same model, again for both flat SFR and the two-infall model. Observed C abundances are taken from Chiappini et al. (2003), Reddy et al. (2003),

Bensby & Feltzing (2006) and Fabbian et al. (2009), O abundances from Gratton et al. (2003), Reddy et al. (2003) and Calura et al. (2010). While early  $[\text{C}/\text{Fe}]$ -values seem to lie slightly too high, and the decreasing trend between  $[\text{Fe}/\text{H}] = -0.5$  and 0 suggested by observations is not reproduced, the models are certainly not incompatible with them. As mentioned before, the early evolution ( $[\text{Fe}/\text{H}] < -1.5$ ) of both elements can be greatly modified by making different assumptions about direct black hole formation and hypernova yields, but this does not affect the G-dwarf metallicity distribution which is the object of this study.

As a final step, the fraction of Fe in the solar neighborhood originating from SNe Ia is investigated. Fig. 13 shows its evolution as a function of time, for the constant SFR, respectively two-infall model calculations. Between 65 and 70% of the Fe present in the solar neighborhood today was created by SNe Ia.

### 3.3. Other considerations

As mentioned in the Introduction, concurrent with this study a comparison has been made by Toonen et al. (2013) between different binary population synthesis models. This exercise has brought to light a number of ingredients, other than intended parameterizations, which may have a profound influence on the outcome of the evolution of a certain system. We will now investigate their consequences for the results obtained so far. A first point is the wind mass loss during the AGB phase. Its yields as computed by van den Hoek & Groenewegen (1997) are included in the code. However, we do not follow the angular momentum loss as a result of these winds in detail. Instead, the mass decrease from TAMS to post-mass transfer phase (i.e. the C-O core) and the resulting orbital separation variation is calculated in one step, thus in fact acting as if this mass is lost in the CE. Of course, this results in a different orbital separation for individual systems as in those codes which follow the AGB phase in detail throughout at the expense of more computation time. However, the effect of this simplification on the eventual DTDs (and thus also the G-dwarf metallicity distributions) has been found to be negligible. The same is true for the simplification of not following in detail the convective core mass evolution between systems filling their Roche lobe early and late on the AGB.

It is important to remark that the considered mass range of the IMF is of paramount importance to the obtained absolute rate of SNe Ia in theoretical studies. If the lower limit of the IMF is taken at about  $0.1 M_{\odot}$  (as most IMFs actually prescribe), then a large portion of the total mass of a starburst is “locked” in low mass systems that do not have a chance to ever result in a SN Ia (or even return their mass to the interstellar medium in any way). If, however, one takes the lower limit at  $1.0 M_{\odot}$ , the contribution to the total mass of the starburst of those systems that are too light to ever be able to produce a SN Ia is significantly reduced, and the SN Ia rate expressed in SNum (events per formed stellar mass) increases. It is well known that most theoretical studies produce absolute SN Ia rates that are up to an order of magnitude lower than the rates that are being observed. One could thus be tempted to use an adapted IMF range to alleviate this problem. However, this should not be done unless there are indications that the observationally studied populations have a low (or even zero) contribution of low mass stars, which is not the case.

#### 4. Conclusions

We have tested the ability of the two most popular type Ia supernova progenitor scenarios, the single and double degenerate channel, to theoretically reproduce the observed indicators of the chemical history of the solar neighborhood. In particular, the metallicity distribution of G-type dwarfs (i.e. the prevalence of such stars with respective iron content) is such an indicator, which is additionally critically affected by the type Ia supernova rate throughout the history of the Galaxy, and thus by the assumptions about their progenitors. This was done by the combination of a population synthesis code including detailed binary evolution and a galactic chemical evolution model. We applied various assumptions and parameters concerning both binary and galactic evolution. Additionally, we updated and extended the study by Mennekens et al. (2010) concerning the ability of both progenitor scenarios to reproduce the observed type Ia supernova delay time distribution (the evolution of the number of such events as a function of time after starburst) in passively evolving elliptical galaxies.

We conclude that both the delay time distribution and the G-dwarf metallicity distribution point towards a significant contribution by both the single degenerate and double degenerate channel. The ability of either traditional progenitor scenario to be solely responsible for all type Ia supernova induced iron enrichment is ruled out. The best match with the observed G-dwarf metallicity distribution (and other galactic observables) is found when assuming that all double C-O white dwarf mergers explode as type Ia supernovae, as well as using a slightly larger convective core mass to account for rotational effects. In addition, the critical dependence of both distributions on certain binary and galactic evolutionary processes, exactly those processes which are modeled with still uncertain parameters in population synthesis studies, is a way to learn more about these processes and thus further constrain these parameters. In particular, we find that most double degenerate type Ia supernova progenitors need to go through a quasi-conservative, stable Roche lobe overflow phase, followed by a common envelope evolution. On a galactic level, a satisfying reproduction of the G-dwarf metallicity distribution requires a high binary frequency and a star formation rate that is relatively constant in time.

*Acknowledgements.* We thank Ivan Ramírez for a useful discussion regarding our comparison with observational AMRs.

#### References

- Abt, H. 1983, *ARA&A*, 21, 343  
 Badenes, C. & Maoz, D. 2012, *ApJ*, 749, L11  
 Belczyński, K., Mikołajewska, J., Munari, U., Ivison, R. & Friedjung, M. 2000, *A&AS*, 146, 407  
 Bensby, T. & Feltzing, S. 2006, *MNRAS*, 367, 1181  
 Calura, F., Recchi, S., Matteucci, F. & Kroupa, P. 2010, *MNRAS*, 406, 1985  
 Cappellaro, E. 1996, *IAUS*, 171, 81  
 Casagrande, L., Schönrich, R., Asplund, M. et al. 2011, *A&A*, 530, A138  
 Chiappini, C., Matteucci, F. & Gratton, R. 1997, *ApJ*, 477, 765  
 Chiappini, C., Matteucci, F. & Meynet, G. 2003, *A&A*, 410, 257  
 Chiosi, C. 1980, *A&A*, 83, 206  
 Chomiuk, L., Soderberg, A., Moe, M., et al. 2012, *ApJ*, 750, 164  
 Claeys, J., Pols, O., Vink, J. & Izzard, R. 2010, *AIPC*, 1314, 262  
 Darwin, G. 1879, *Phil. Trans. Roy. Soc.*, 170, 447  
 Davis, P., Kolb, U. & Willems, B., 2010, *MNRAS*, 403, 179  
 De Donder, E. & Vanbeveren, D. 2003, *NewA*, 8, 415  
 De Donder, E. & Vanbeveren, D. 2004, *NewAR*, 48, 861  
 De Greve, J.P. & De Loore, C. 1976, *Ap&SS*, 43, 35  
 Delgado, A. & Thomas, H. 1981, *A&A*, 96, 142  
 Dewi, J. & Tauris, T. 2000, *A&A*, 360, 1043  
 Fabbian, D., Nissen, P., Asplund, M., Pettini, M. & Akerman, C. 2009, *A&A*, 500, 1143  
 Garmany, C., Conti, P. & Massey, P. 1980, *ApJ*, 242, 1063  
 Gratton, R., Carretta, E., Claudi, R., Lucatello, S. & Barbieri, M. 2003, *A&A*, 404, 187  
 Greggio, L., Renzini, A. & Daddi, E. 2008, *MNRAS*, 388, 829  
 Hachisu, I., Kato, M. & Nomoto, K. 1999, *ApJ*, 522, 487  
 Hachisu, I., Kato, M. & Nomoto, K. 2008, *ApJ*, 679, 1390  
 Hachisu, I., Kato, M., Saio, H. & Nomoto, K. 2012, *ApJ*, 744, 69  
 Han, Z. & Podsiadlowski, P. 2004, *MNRAS*, 350, 1301  
 Heger, A. & Woosley, S. 2002, *ApJ*, 567, 532  
 Hogeveen, S. 1992, *Ap&SS*, 196, 299  
 Holmberg, J., Nordström, B. & Andersen, J. 2007, *A&A*, 475, 519  
 Hurley, J., Tout, C. & Pols, O. 2002, *MNRAS*, 329, 897  
 Iben, I., Jr. & Tutukov, A. 1984, *ApJS*, 54, 335  
 Ilkov, M. & Soker, N. 2012a, *MNRAS*, 419, 1695  
 Ilkov, M. & Soker, N. 2012b, *MNRAS*, in press (arXiv:1208.0953)  
 Iwamoto, K., Brachwitz, F., Nomoto, K. et al. 1999, *ApJS*, 125, 439  
 Kashi, A. & Soker, N. 2011, *MNRAS*, 417, 1466  
 Kobayashi, C. & Nakasato, N. 2011, *ApJ*, 729, 16  
 Kobayashi, C., Tsujimoto, T., Nomoto, K., Hachisu, I. & Kato, M. 1998, *ApJ*, 503, 155  
 Kroupa, P., Tout, C. & Gilmore, G. 1993, *MNRAS*, 262, 545  
 Lee, Y. S., Beers, T., An, D. et al. 2011, *ApJ*, 738, 187  
 Mannucci, F., Della Valle, M., Panagia, N. et al. 2005, *A&A*, 433, 807  
 Maoz, D. & Mannucci, F. 2012, *PASA*, 29, 447  
 Maoz, D., Mannucci, F. & Brandt, T. 2012, *MNRAS*, 426, 3282  
 Matteucci, F., Spitoni, E., Recchi, S. & Valiante, R. 2009, *A&A*, 501, 531  
 Mennekens, N., Vanbeveren, D., De Greve, J.P. & De Donder, E. 2010, *A&A*, 515, A89 (M10)  
 Nakamura, T., Umeda, H., Iwamoto, K. et al. 2001, *ApJ*, 555, 880  
 Nelemans, G., Verbunt, F., Yungelson, L. & Portegies Zwart, S. 2000, *A&A*, 360, 1011  
 Neo, S., Miyaji, S., Nomoto, K. & Sugimoto, D. 1977, *PASJ*, 29, 249  
 Nomoto, K. 1982, *ApJ*, 253, 798  
 Packet, W. 1981, *A&A*, 102, 17  
 Paczyński, B. 1967, *AcA*, 17, 193  
 Pakmor, R., Kromer, M., Röpke, F. et al. 2010, *Nature*, 463, 61  
 Piersanti, L., Gagliardi, S., Iben, I., Jr. & Tornambé, A. 2003, *ApJ*, 583, 885  
 Podsiadlowski, P., Joss, P. & Hsu, J. 1992, *ApJ*, 391, 246  
 Ramírez, I., Allende Prieto, C. & Lambert, D. 2007, *A&A*, 465, 271  
 Rana, N. 1991, *ARA&A*, 29, 129  
 Rappaport, S., Verbunt, F. & Joss, P. 1983, *ApJ*, 275, 713  
 Reddy, B., Tomkin, J., Lambert, D. & Allende Prieto, C. 2003, *MNRAS*, 340, 304  
 Roškar, R., Debattista, V., Quinn, T., Stinson, G. & Wadsley, J. 2008, *ApJ*, 684, L79  
 Ruiter, A., Belczynski, K., Sim, S. et al. 2011, *MNRAS*, 417, 408  
 Schaefer, B. & Pagnotta, A. 2012, *Nature*, 481, 164  
 Soberman, G., Phinney, E. & van den Heuvel, E. 1997, *ApJ*, 327, 620  
 Talbot, R. & Arnett, W. 1975, *ApJ*, 197, 551  
 Toonen, S., Nelemans, G. & Portegies Zwart, S. 2012, *A&A*, 546, A70  
 Toonen, S., Claeys, J., Mennekens, N. & Ruiter, A. 2013, *A&A*, in preparation  
 Totani, T., Morokuma, T., Oda, T., Doi, M. & Yasuda, N. 2008, *PASJ*, 60, 1327  
 van den Hoek, L. & Groenewegen, M. 1997, *A&AS*, 123, 305  
 van Kerkwijk, M., Chang, P. & Justham, S. 2010, *ApJ*, 722, L157



- Vanbeveren, D. & De Loore, C. 1994, *A&A*, 290, 129
- Vanbeveren, D. & De Donder, E. 2006, *NewA*, 12, 95
- Vanbeveren, D., Van Rensbergen, W. & De Loore, C. 1998a, *A&AR*, 9, 63
- Vanbeveren, D., De Donder, E., Van Bever, J., Van Rensbergen, W. & De Loore, C. 1998b, *NewA*, 3, 443
- Wang, B., Chen, X., Meng, X. & Han, Z. 2009, *ApJ*, 701, 1540
- Webbink, R. 1984, *ApJ*, 277, 355
- Whelan, J. & Iben, I., Jr. 1973, *ApJ*, 186, 1007
- Woosley, S. & Weaver, T. 1995, *ApJS*, 101, 181
- Zorotovic, M., Schreiber, M., Gänsicke, B. & Nebot Gómez-Morán, A. 2010, *A&A*, 520, A86